IEEE Access
Multidisciplinary | Rapid Review | Open Access Journal

Received July 30, 2019, accepted August 29, 2019, date of publication September 11, 2019, date of current version September 20, 2019.

*Digital Object Identifier 10.1109/ACCESS.2019.2940299*

# Non-Orthogonal Multicarrier Waveform for Radar With Communications Systems: 24 GHz GFDM RadCom

**JESSICA B. SANSON[1,2], (Student Member, IEEE), DANIEL CASTANHEIRA[2], ATÍLIO GAMEIRO[1,2], AND PAULO P. MONTEIRO[1,2], (Senior Member, IEEE)**

[1]DETI, University of Aveiro, 3810-193 Aveiro, Portugal
[2]Instituto de Telecomunicações, 3810-193 Aveiro, Portugal

Corresponding author: Jessica B. Sanson (jessica.sanson@ua.pt)

This work was supported by the European Regional Development Fund through the Competitiveness and Internationalization Operational Program, Regional Operational Program of Lisbon, Regional Operational Program of the Algarve, in componente FEDER, and the Foundation for Science and Technology, Project, RETIOT, POCI-01-0145-FEDER-016432. The work of J. Sanson was supported by Foundation for Science and Technology under Ph.D. Grant PD/BD/128195/2016.

**ABSTRACT** In this paper, we propose the usage of Generalized Frequency Division Multiplexing (GFDM), a non-orthogonal multicarrier waveform for radar. We presented a novel method that cancels the effect of interference caused by the non-orthogonality of GFDM waveform in the radar processing, thus not affecting the performance of the radar. We show the viability of GFDM for radar with communications systems and the benefits of using it over Orthogonal Frequency Division Multiplexing (OFDM). Finally, we also present GFDM as a solution to mitigate inter-system interference in radar with communications (RadCom) systems, thus showing that GFDM may prove to be a better candidate than OFDM for RadCom applications. This method is validated with simulations and practical measurements at 24 GHz.

**INDEX TERMS** GFDM, matched filter, non-orthogonal, OFDM radar, RadCom.

## I. INTRODUCTION

Combined radar/communications systems (RadCom) use the same hardware and signals to perform target detection and communication simultaneously. By integrating radar and communication functionalities into one single device, these systems are expected to provide advantages in terms of cost, size and occupied spectrum. RadCom systems have the potential to be employed for area surveillance, search and rescue, and intelligent transportation.

The integration of radar and communications will be important for beyond 5G systems where a radar component will add a sensing component to a telecommunication network. In fact, different technologies and applications can use integrated communication and radar signals. In [1]–[3] for example, passive radars are used for air, vehicular and even naval traffic control. The use of communication signals for synthetic aperture radar (SAR) was considered in [4], [5]. In [6]–[8], the authors used intrapulse radar-embedded communication procedure based on the remodulation of the incident radar signaling, in covert communication for defence-related application. The use of communication signals of mobile personal devices operating as mobile radars for internal mapping has been proposed in [9]. In [10], the use of radar and communication with the same signal for vehicles are considered in transportation systems.

The use of Orthogonal Frequency Division Multiplexing (OFDM) for radar was first proposed in [11], and preliminary studies of the integration of radar and communication functionalities were carried out in [12]. A major step in the implementation of RadCom systems was presented in [13], where a more efficient and simpler radar processing algorithm was proposed—the direct processing of the modulated symbols instead of the baseband signal. A review of RadCom technology is provided in [14].

OFDM is a well-known waveform that has been extensively studied for the joint radar and communication applications [1], [2], [4], [15]–[19]. OFDM has some disadvantages, however, such as high out-of-band (OOB) emission, susceptibility to Doppler spread, loss of spectral efficiency due to the use of a cyclic prefix (CP), and the need for frequency synchronization to preserve the orthogonality of the subcarriers [20]. In RadCom systems, the disadvantages of the OFDM waveform affect not only the communications functions but

The associate editor coordinating the review of this manuscript and approving it for publication was Pia Addabbo.


This work is licensed under a Creative Commons Attribution 4.0 License. For more information, see http://creativecommons.org/licenses/by/4.0/

also the radar. For example, in order to compensate for strong OOB emission in OFDM, guard bands are required, which decrease the range resolution of the radar.

To overcome some of the limitations of OFDM in communications systems, several alternative candidates waveforms have been proposed, such as Universal Filtered Multicarrier (UFMC), Generalized Frequency Division Multiplexing (GFDM) and Filter Bank Multicarrier (FBMC) [21]. UFMC, although better contained than OFDM, has higher out-of-band emissions than GFDM and FBMC [22]. FBMC is a spectrally well-contained waveform, with a very high computational complexity [23] and its use for radar was considered in [24], [25]. In [24], the authors consider the use of offset quadrature amplitude modulation (OQAM) FBMC for radar as an extension of OFDM. However, the non-orthogonality subjacent to the OQAM modulation introduces interference in the radar estimates. In [25], the authors use non-offset QAM instead of OQAM. However, the use of the QAM modulation in FBMC increases the computational complexity.

Generalized Frequency Division Multiplexing (GFDM) is a flexible and well-contained spectral multicarrier modulation with low computational complexity [26]–[28]. GFDM is a block-based multicarrier transmission scheme. The processing of these blocks is based on digital filters that preserve the circular properties of the signals over the time and frequency domains [29]. This process reduces OOB emission, making possible the use of spectrum without severely interfering with established services or other users [30].

In GFDM, the transmission data of each block are distributed in time and frequency, and the insertion of CP is done in each block. This increases the spectral efficiency while still providing the means for efficient channel equalization [31]. GFDM blocks are independent of each other, with a structure shaped as desired, so it is possible to adaptively design their structure in order to match the limitations of time and system latency [32]. For example, in real-time applications, the signal length may be reduced to operate under low-latency requirements [30], [33], which makes it an attractive option for applications such as the Internet of Things and radar [26]. Furthermore, GFDM can be easily implemented in multiple-input multiple-output (MIMO) systems [30]. Previous studies have already shown the superiority of the use of GFDM for vehicular communications in relation to OFDM. In [34], it is demonstrated that GFDM can utilize the time and frequency resources more efficiently than OFDM and outperform it particularly under challenging channel conditions for intelligent transportation systems. Motivated by these attractive features, in this paper, we present a method for radar processing with GFDM, demonstrating the viability of its use in RadCom systems and its benefits over OFDM. We also present GFDM as a solution to mitigate inter-system interference in RadCom systems.

This paper is organized as follows. In Section II, we establish a common system model for the processing of multicarrier radar and as a special case, we present the OFDM radar model. In Section III, we provide a brief outline of the GFDM modulation scheme, from the viewpoint of communication systems. In Section IV, the proposed method for radar processing with GFDM waveforms is described. In Section V, the laboratory setup and measurements of a 24 GHz RadCom system are detailed. In Section VI, we present the evaluation of the performance of the proposed GFDM radar system for two distinct scenarios: one with a single user, where the resolution capacity of the system is analyzed, and another with multiple users, where an evaluation of the interference between users (inter-system interference) is performed. Finally, in Section VII we present our conclusions.

*Notation:* In this paper, bold lower-case letters denote vectors and bold upper-case letters denote matrices. The following mathematical symbols have also been used:

| | |
|---|---|
| $(\cdot)^T$ | Transpose, |
| $(\cdot)^H$ | Conjugate transpose, |
| $\mathbf{I}_K$ | $K \times K$ Identity matrix, |
| $\|\cdot\|$ | Euclidean norm, |
| rect$(\cdot)$ | Rectangular function, |
| circshift$\{\cdot, k\}$ | Circular shift of $k$, |
| $k$ mod $K$ | Modulus after division of $k$ by $K$, |
| $\circledast$ | Circular convolution, |
| $vec\{\cdot\}$ | Vector operator, |
| $res\{\cdot\}_{K\times L}$ | Reshaping vector of size $KL$ in a $K \times L$ matrix, |
| DFT$(\cdot)$ | Discrete Fourier transform, |
| IDFT$(\cdot)$ | Inverse discrete Fourier transform. |

## II. SYSTEM MODEL

In this paper we consider a RadCom system in which the information to be transmitted is encoded by a digital complex-modulation technique; the encoded data is represented by the data matrix $\mathbf{S}$. The data matrix $\mathbf{S}$ is transmitted by the RadCom System using a multicarrier modulation technique. The transmitted signal is then reflected by the targets and received back by the same RadCom system. As far as radar functionality is concerned, the received data sequence is known in advance. An example scenario with vehicles equipped with and without RadCom systems as depicted in Fig. 1, where an arbitrary vehicle transmits the RadCom signal and receives this signal reflected by the targets. This vehicle can also communicate with other devices (e.g. other vehicles).

### A. BASIC MULTICARRIER RADAR

Consider a radar system with a multicarrier modulation signal represented by a matrix of complex data symbols distributed in the time and frequency domains, with $N$ subcarriers and $M$ multicarrier symbols. The complex envelope of the transmitted time-domain signal can be expressed by

$$x(t) = \sum_{m=0}^{M-1} \sum_{n=0}^{N-1} S(n, m) g(t - mT) e^{j2\pi n \Delta f t}, \qquad (1)$$

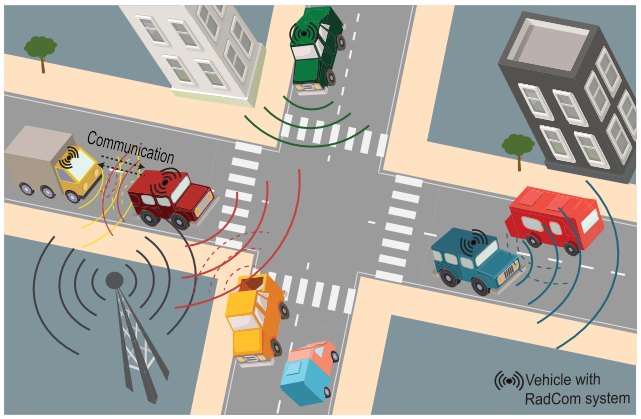


**FIGURE 1.** Example scenario with vehicles equipped with and without RadCom systems (reflected/transmittred wave - dashed/undashed curve).

where $\Delta f$ is the subcarrier spacing, $T$ is the duration of one multicarrier symbol and $g(t)$ is the filter impulse response used to modulate the symbols.

In the presence of a reflective target $\omega$ at a distance $R_\omega$ of the RadCom system and a relative velocity of $v_\omega$, the received signal has a time delay of $2R_\omega/c$ and a frequency shift of $f_{D\omega} = 2\, f_c v_\omega/c$, where $c$ is the speed of light and $f_c$ is the carrier frequency. Then being reflected by $\Omega$ targets, the received signal becomes [13]

$$y(t) = \sum_{\omega=1}^{\Omega} \sum_{m=0}^{M-1} \sum_{n=0}^{N-1} S(n,m) g(t - mT) e^{j2\pi f_{D\omega} t} e^{j2\pi n \Delta f (t - \frac{2R_\omega}{c})} + \eta(t), \quad (2)$$

and using the conversion of the time-domain signal to the discrete form by $t = kT/N = k/(N\Delta f)$ (according to the Nyquist sampling criterion), where $k$ is the sample index, the discrete-time form becomes

$$y(k) = \sum_{\omega=1}^{\Omega} \sum_{m=0}^{M-1} \sum_{n=0}^{N-1} S(n,m) g\left(\frac{k}{N\Delta f} - mT\right) e^{j2\pi f_{D\omega} mT} e^{\frac{j2\pi kn}{N}} e^{-j2\pi n \Delta f \frac{2R_\omega}{c}} + \eta(k), \quad (3)$$

where $\eta$ is the time-domain complex additive white Gaussian noise (AWGN) and $k = 0, \ldots, NM-1$. After demodulation, the estimated received signal $\hat{\mathbf{S}}$ is then used to estimate the delay and Doppler shift of the targets. This estimation is performed by comparing the transmitted symbols $\mathbf{S}$ with the received symbols $\hat{\mathbf{S}}$, generating the frequency-domain channel transfer matrix $\mathbf{D}$ [13] with elements defined by

$$D(n,m) = \frac{\hat{S}(n,m)}{S(n,m)}. \quad (4)$$

The range and velocity parameters can be obtained from a two-dimensional DFT (2D-DFT) [13]: the DFT of length $M$ in each line of $\mathbf{D}$ and the IDFT of length $N$ in each column

$$\mathbf{Z} = \text{IDFT}[\text{DFT}[\mathbf{D}]]. \quad (5)$$

The range resolution [35] of the radar is

$$\Delta R = \frac{c}{2B} = \frac{c}{2N\Delta f} = \frac{cT}{2N}, \quad (6)$$

where $B$ is the signal bandwidth. The resolution needs to be small enough to allow the separation of objects such as cars, buildings, etc. [13]. The velocity resolution depends on the total duration of evaluated symbols $T_F$ [35], being

$$\Delta v = \frac{c}{2T_F f_c}. \quad (7)$$

The maximum unambiguous velocity and the maximum measurement distance are $v_{max} = c/(2\, f_c T)$ and $R_{max} = c/(2\Delta f)$ respectively.

### B. OFDM RADAR

In an OFDM system the filter $g(t)$ is a rectangular pulse of lenght $T_{OFDM}$. The use of this pulse ensures orthogonality between sub-carriers. The OFDM signal is generated by applying an IDFT of length $N$ to the modulated symbols. The complex envelope of the transmitted time-domain OFDM signal is expressed by

$$x(t) = \sum_{m=0}^{M-1} \sum_{n=0}^{N-1} S(n,m) e^{j2\pi n \Delta f t} \text{rect}\left(\frac{t - mT}{T}\right), \quad (8)$$

With $T_{OFDM} = T + T_{CP}$ being the total OFDM symbol duration composed of an elementary symbol duration $T$ and a cyclic prefix (CP) duration $T_{CP}$.

At the receiver, the symbols are demodulated using a DFT of length $N$. Thus, the estimated symbols received by the OFDM radar are defined as

$$\hat{S}(n,m) = \sum_{\omega=1}^{\Omega} S(n,m) e^{j2\pi f_{D\omega} m T_{OFDM}} e^{-j2\pi n \Delta f \frac{2R_\omega}{c}} + \tilde{\eta}(n,m), \quad (9)$$

where $\tilde{\eta}$ is the frequency-domain AWGN. In this system, the cyclic prefix (CP) is inserted at the beginning of each transmitted OFDM symbol (after applying the IDFT). During reception, the CP is discarded before the signal is demodulated. In OFDM radar the total duration of evaluated symbols is $T_F = MT_{OFDM} = M(T + T_{CP})$.

## III. REVIEW OF GFDM IN COMMUNICATIONS SYSTEMS

In this section, we present the GFDM waveform and corresponding transceiver, from the viewpoint of a communication system, shown in Fig. 2. The use of the GFDM waveform for the radar functionality is presented in the following section.

The GFDM block is composed of $N$ subcarriers and $M$ symbols and contains $K = NM$ complex data symbols. The duration of a GFDM block is $T_{GFDM} = MT + T_{CP}$, where $T = 1/\Delta f$ is the duration of an elementary symbol.

The details of the GFDM modulator are shown in Fig. 3 [30]. Each GFDM symbol is filtered by its corresponding pulse-shaping filter, which is implemented based on a prototype $p[k]$ filter with an offset in time and in frequency, as shown in Fig. 3 [36].

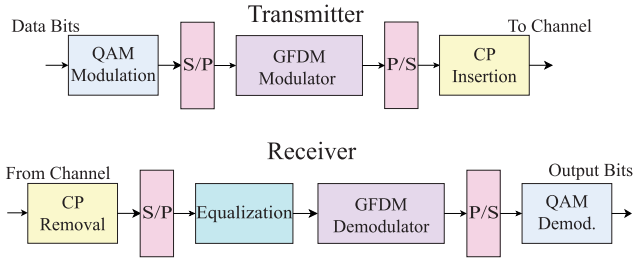


**FIGURE 2.** GFDM transceiver.

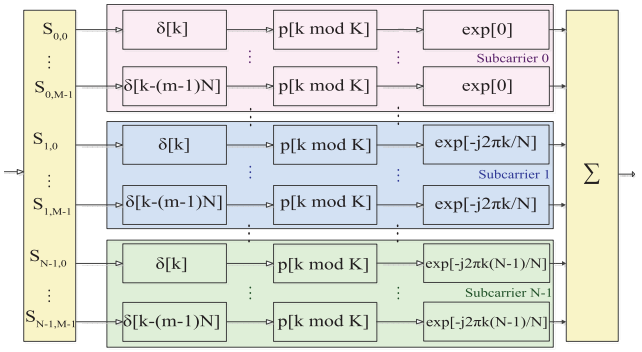


**FIGURE 3.** GFDM modulator.

The subcarrier filtering performed in GFDM results in non-orthogonal subcarriers, which leads to inter-carrier (ICI) and inter-symbol interference (ISI), denominated by intrinsic interference in the following. Different filters can be used to filter subcarriers, and this choice affects OOB emissions and intrinsic interference [30]. To avoid inter-symbol interference, a CP is added at the beginning of each block of symbols instead of each symbol as in OFDM [21], as shown in Fig. 4.

In the receiver, the CP is first removed and each block is equalized to remove the intrinsic interference caused by the non-orthogonality between subcarriers. After equalization, each block is filtered by the same time and frequency translated filters that were used in the transmission stage [30].

The structure of the complex data matrix $\mathbf{S}$ in a GFDM block is

$$\mathbf{S} = \begin{bmatrix} S(0,0) & \dots & S(0,M-1) \\ \vdots & \ddots & \vdots \\ S(N-1,0) & \dots & S(N-1,M-1) \end{bmatrix} \quad (10)$$

and the transmitted GFDM signal [30] can be expressed as

$$x(k) = \sum_{m=0}^{M-1} \sum_{n=0}^{N-1} S(n,m) p[(k-mN) \bmod K] e^{\frac{j2\pi kn}{N}}, \quad (11)$$

with $k = 0, \dots, K-1$. The corresponding pulse shaping filter is

$$p_{n,m}[k] = p[(k-mN) \bmod K] e^{\frac{j2\pi kn}{N}}. \quad (12)$$

Each $p_{n,m}[k]$ is a circularly shifted version of $p_{n,0}[k]$, and the complex exponential performs the frequency shift operation [30].

The transmitted samples can then be represented by

$$x(k) = \sum_{m=0}^{M-1} \sum_{n=0}^{N-1} S(n,m) p_{n,m}[k]. \quad (13)$$

This equation can be rearranged in matrix form,

$$\mathbf{x} = \mathbf{A} vec\{\mathbf{S}\}, \quad (14)$$

where $\mathbf{x} = [x[1], \dots, x[K]]^T$ is the $K \times 1$ transmitted signal, $\mathbf{A}$ is a $K \times K$ modulation matrix [30] with a structure according to

$$\mathbf{A} = [\mathbf{p}_{0,0} \quad \dots \quad \mathbf{p}_{N-1,0}, \quad \mathbf{p}_{0,1} \quad \dots \quad \mathbf{p}_{N-1,M-1}], \quad (15)$$

with the vector $\mathbf{p}_{n,m} = [p_{n,m}[1], \dots, p_{n,m}[K]]^T$. The received signal vector can be defined as

$$\mathbf{y} = \mathbf{H_C}\mathbf{x} + \boldsymbol{\eta}, \quad (16)$$

where $\boldsymbol{\eta}$ is a complex AWGN vector. The channel matrix $\mathbf{H_C}$ of size $K \times K$ is a circular convolution matrix and each column of the matrix [26] is given by the circular shift of the channel impulse response $\mathbf{h}$ with the length (in samples) of $L_c$

$$[\mathbf{H_C}]_{(:,k)} = \text{circshift}\left\{[h_0, \cdots, h_{L_c-1}, \mathbf{0}_{K-L_c}]^T, k-1\right\}. \quad (17)$$

In the receiver of the communications system, the zero forcing equalizer ($\mathbf{H_C}^{-1}$) can be used for channel equalization, although other procedures can be employed. As detailed in [30], the estimated received data matrix $\hat{\mathbf{S}}$ can be obtained by

$$\hat{\mathbf{S}} = res\{\mathbf{C}\mathbf{H_C}^{-1}\mathbf{y}\}_{N \times M}, \quad (18)$$

where $\mathbf{C}$ is the $K \times K$ demodulation matrix of GFDM, which can be, e.g., the matched filter (MF), zero forcing (ZF), or minimum mean square error (MMSE) matrices [30], defined below

$$\mathbf{C}_{MF} = \mathbf{A}^H, \quad (19)$$

$$\mathbf{C}_{ZF} = \mathbf{A}^H(\mathbf{A}\mathbf{A}^H)^{-1}, \quad (20)$$

$$\mathbf{C}_{MMSE_H} = \left(\mathbf{A}^H \mathbf{H_C}^H \mathbf{H_C} \mathbf{A} + \mathbf{R}_\eta^2\right)^{-1} \mathbf{A}^H \mathbf{H_C}^H. \quad (21)$$

where $\mathbf{R}_\eta^2$ is the covariance matrix of the noise. Note that in case of MMSE reception, the channel is jointly equalized in the receiving process.

## IV. GFDM RADAR

The signal received by the radar, assuming that we have $\Omega$ reflective targets and $M_B$ GFDM blocks, is given by

$$y[k] = \sum_{\omega=1}^{\Omega} \sum_{b=0}^{M_B-1} \sum_{m=0}^{M-1} \sum_{n=0}^{N-1} S_b(n,m) p_{n,m}[k] \, e^{j2\pi f_{D\omega}(Tm+T_{GFDM}b)} e^{-j2\pi n\Delta f \frac{2R_\omega}{c}} + \tilde{\eta}(m,n). \quad (22)$$

where $S_b$ is the data matrix of the GFDM block $b$, with $b = 0, \dots, M_B - 1$. The total duration of evaluated symbols in GFDM radar is $T_F = M_B T_{GFDM} = M_B(MT + T_{CP})$

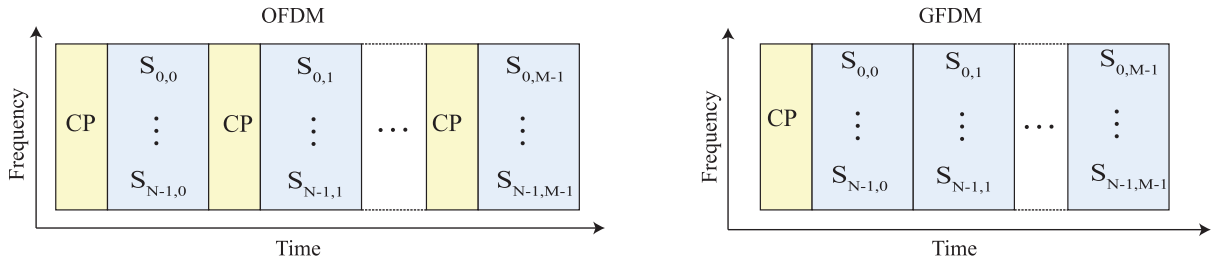


**FIGURE 4.** Structure of OFDM and GFDM signals composed of *N* subcarriers and *M* symbols.

For the estimation of the matrix of received symbols in the radar, contrary to the processing in communications systems, we remove the channel equalization matrix $\mathbf{H_C}^{-1}$ in (18) in order to preserve the information from the channel. The estimated received symbols are then obtained as

$$\hat{\mathbf{S}}^{\dagger} = res\{\mathbf{Cy}\}_{N\times M}. \tag{23}$$

In the radar receiver, the demodulation matrix $\mathbf{C}$ of GFDM needs to be properly chosen. The influence of the shape of the filtered pulse in GFDM leads to a non-orthogonality condition causing inter-symbol and inter-carrier interference in the received symbols. This interference was denominated by intrinsic interference in the previous section.

The use of the MF for the demodulation maximizes the signal-to-noise ratio (SNR) per subcarrier but does not remove the intrinsic interference. The ZF receiver, on the other hand, removes the intrinsic interference at the cost of decreasing the SNR. In addition, there may be instances where $\mathbf{A}$ is poorly conditioned, further deteriorating the SNR. The linear MMSE receiver makes a trade-off between intrinsic interference and noise suppression. However, in the case of MMSE, the channel is equalized together in the receiving process, which impairs the estimation of radar targets. For these reasons, MF and ZF are suitable for radar processing, while MMSE is not [30].

### A. GFDM - ZF/MF RADAR

Considering the cases of GFDM radar with ZF receiver (GFDM-ZF), and GFDM radar with MF (GFDM-MF) receiver, the radar processing is performed directly with the matrix of transmitted symbols $\mathbf{S}^{\dagger}_{ZF/MF} = \mathbf{S}$, as well as in OFDM. The estimated received symbols are $\hat{\mathbf{S}}^{\dagger}_{ZF/MF} = res\{\mathbf{C}_{ZF/MF}\mathbf{y}\}_{N\times M}$ and then components of estimation matrix $\mathbf{D}$ are

$$D(m+Mb,n) = \frac{\hat{S}^{\dagger}_{b,ZF/MF}(m,n)}{S^{\dagger}_{b,ZF/MF}(m,n)}. \tag{24}$$

### B. GFDM - PMF RADAR

To overcome the aforementioned problems of ZF and MF in GFDM based radar, we propose an intrinsic interference cancelation technique based on the MF approach for GFDM radar (denoted by GFDM-PMF). This technique cancels the intrinsic interference in the matrix $\mathbf{D}$ without increasing the background noise, as occurs with GFDM-ZF. Concerning the radar functionalities, our GFDM-PMF allows the optimum performance. The details are presented in the appendix, but basically the technique resort to the fact that for MF in (24), $\hat{\mathbf{S}}^{\dagger}_{MF}$ can be decomposed as interference, noise and intended signal while in the denominator we just have the intended signal. The PMF technique estimates the interference complement and adds it in the denominator. Although we have no interblock interference, inside the blocks the waveforms are non-orthogonal. For all interference between the symbols and subcarrier to be removed, it is necessary to consider the whole GFDM block in the radar processing.

In GFDM-PMF, the MF receiver (the $\mathbf{C}_{MF}$ matrix) is used for the estimation of the received symbols $\hat{\mathbf{S}}^{\dagger}_{PMF}$, therefore

$$\hat{\mathbf{S}}^{\dagger}_{PMF} = res\{\mathbf{C}_{MF}\mathbf{y}\}_{N\times M}. \tag{25}$$

The matrix $\mathbf{S}$ is processed in order to estimate the intrinsic interference suffered by the transmitted symbols. This estimation is done by applying the same filtering process the received symbols went through (the two pulse-shaping filters of the transmit and receive stages, $\mathbf{A}$ and $\mathbf{A}^H$) to the transmitted symbols ($\mathbf{S}$, cf. the appendix). This results in a matrix $\mathbf{S}^{\dagger}_{PMF}$, defined as

$$\mathbf{S}^{\dagger}_{PMF} = res\{\mathbf{A}^H\mathbf{A}vec\{\mathbf{S}\}\}_{N\times M}, \tag{26}$$

that incorporates not only the transmitted symbols but the intrinsic interference as well. This way, as shown in the appendix, the intrinsic interference is compensated for when computing the radar estimation matrix $\mathbf{D}$.

Considering, then, $M_B$ GFDM blocks evaluated in the radar estimation, the components of estimation matrix $\mathbf{D}$ for GFDM-PMF are

$$D(m+Mb,n) = \frac{\hat{S}^{\dagger}_{b,PMF}(m,n)}{S^{\dagger}_{b,PMF}(m,n)} \tag{27}$$

$$= \sum_{\omega=1}^{\Omega} e^{j2\pi f_{D\omega}(Tm+T_{GFDM}b)} e^{-j2\pi n\Delta f\frac{2R_\omega}{c}} + \tilde{\eta}(m,n). \tag{28}$$

The range and velocity parameters can be obtained from a 2D-DFT as in OFDM radar.

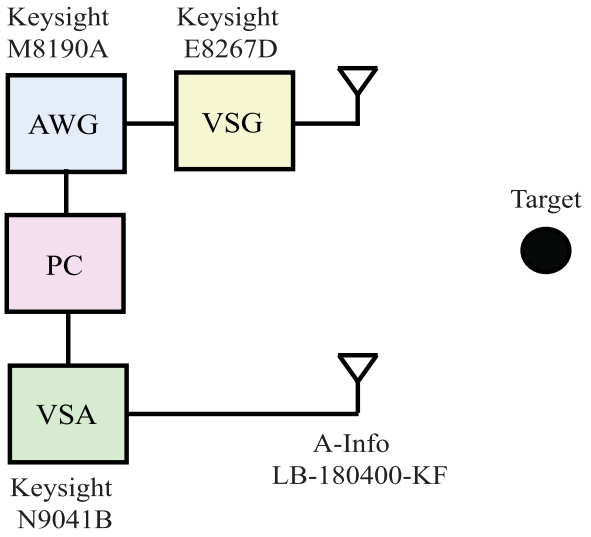


**FIGURE 5.** Diagram of the measurement setup.


**FIGURE 6.** Photograph of the (a) measurement setup, (b) scenario with one target, and (c) scenario with two targets.

## V. RADAR MEASUREMENTS

In this section, we will present the laboratory setup and measurements of a 24 GHz RadCom system, results obtained in the laboratory environment is detailed. In the next section (section VI), we will present results obtained by simulation, in order to complement and validate those obtained in the laboratory.

### A. MEASUREMENT SETUP

The measurement scenario for the 24 GHz radar system was performed in the laboratory and is schematized in Fig. 5. The frequency of 24 GHz was considered due to being the frequency, together with 77GHZ, normally used in automotive radars. The radar system front-end consisted of two A-Info LB-180400-KF 15 dBi horn antennas: one for the transmission and another for the reception. The transmitted data was randomly generated with a 4-QAM constellation. The transmitted waveform (OFDM or GFDM) had a bandwidth of 113.92 MHz and was synthesized in the baseband, at a sample rate of 683.52 MSa/s, using a Keysight M8190A arbitrary waveform generator (AWG). The AWG outputs the in-phase ($I$) and quadrature ($Q$) components of the waveform in a differential-pair configuration ($I/\bar{I}$ and $Q/\bar{Q}$). The baseband waveform was then converted to the 24 GHz band using a Keysight E8267D PSG vector signal generator (VSG). The signal at the output of the VSG had an average power of 14 dBm and was fed to the transmitting antenna.

The signal received by the receiving antenna was measured using a Keysight N9041B UXA vector signal analyzer (VSA). For greater accuracy of measurement, the 10 MHz oscillator of the VSA was used as a reference to synchronize the clocks of all instruments (the AWG, the VSG, and the VSA), and a baseband trigger signal was provided by the AWG to the VSA.

The AWG was connected via USB to a personal computer (PC) and the other instruments were connected through a local area network to the same computer. All instruments were controlled via Matlab, where all signals were generated and processed.

The measurement scenarios are shown in Fig. 6, with one and two targets, respectively. In the first scenario, we have a copper target with $30 \times 22$ cm dimensions at a distance of 2 m (at an angle of 0°) from the radar front-end. In the second scenario, we have two copper targets with 35 × 22 cm and 30 × 22 cm dimensions, at a distance of 3.7 m (0°) and 1.5 m (25°) respectively. Only static targets were considered in these scenarios because no moving targets were available.

Two types of measurements were made: one with a single user (radar) without inter-system interference, and another with two users (two radars) with inter-system interference. For the case with interference between users, two signals were generated with a bandwidth of 113.92 MHz and with different average powers according to the desired signal-to-interference ratio at the radar input ($SIR_{in}$). These signals were allocated to adjacent bands and were synthesized together by the AWG. The received signal (in complex baseband form) was filtered by a sharp low-pass filter in order to select the desired user band. In the multi-user case, the received signal was averaged across 25 consecutive VSA measurements in order to reduce the effects of external noise and to better observe the effects of the inter-system interference. In the single-user case, only one measurement was performed.

The calibration of the system was performed with the transmitting and receiving antennas positioned facing one another at a short distance, thus measuring the total delay of the system (cables, AWG, VSG, VSA and antennas). This delay was then removed from the received signal during radar processing. The transmitting and receiving antennas were 12 cm apart. The coupling between the antennas, measured using a Keysight N5242A Vector Network Analyzer, was below −50 dB in the band of operation, ensuring the leakage interference is negligible.

### B. GFDM RADAR PARAMETERIZATION

Following the parametrization constraints discussed for OFDM RadCom in [35], the parameters for the OFDM radar used in this paper are shown in Table 1. From these parameters, we may find the equivalent ones for the GFDM

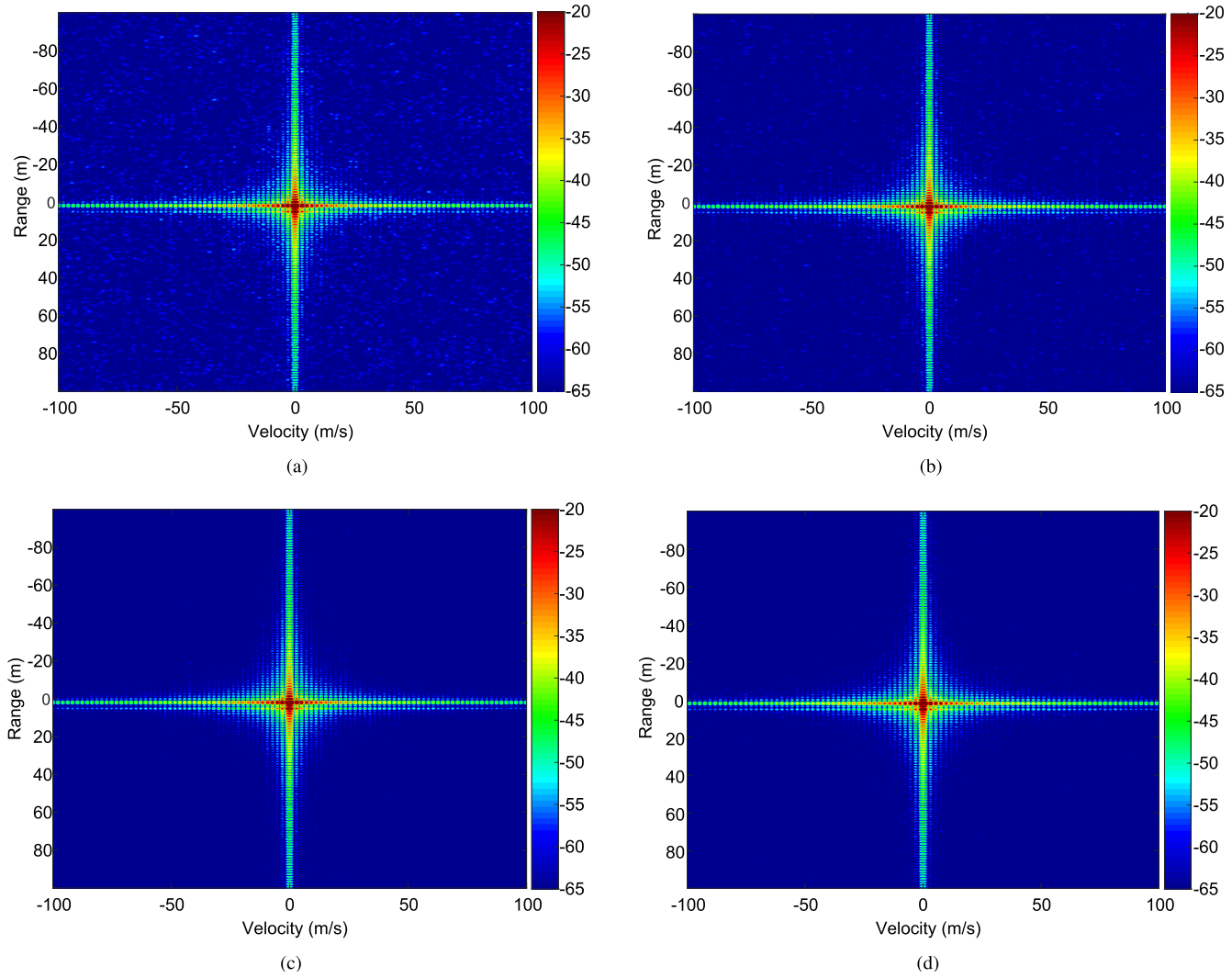


**FIGURE 7.** Radar image for (a) GFDM-MF with intrinsic interference, (b) GFDM-ZF, (c) GFDM-PMF without intrinsic interference, and (d) OFDM.

**TABLE 1.** OFDM system parameters.

| PARAMETERS | SYMBOL | VALUE |
|---|---|---|
| Carrier frequency | $f_c$ | 24 GHz |
| Number of subcarriers | $N$ | 1024 |
| Number of evaluated symbols | $M$ | 256 |
| Total signal bandwidth | $B$ | 113.92 MHz |
| Subcarrier spacing | $\Delta f$ | 111.25 kHz |
| OFDM elementary symbol duration | $T$ | 9.00 $\mu$s |
| Cyclic prefix duration | $T_{CP}$ | 2.25 $\mu$s |
| OFDM symbol duration | $T_{OFDM}$ | 11.25 $\mu$s |
| Duration of evaluated symbols | $T_F$ | 3 ms |
| Range resolution | $\Delta R$ | 1.316 m |
| Velocity resolution | $\Delta v$ | 2.171 m/s |
| Unambiguous range | $R_{max}$ | 1347 m |
| Unambiguous velocity | $v_{max}$ | $\pm$ 278 m/s |
| Modulation | | 4-QAM |

waveform. Note that, in order to maintain the same resolution values (for comparative performance purposes), we maintained the same bandwidth $B$ and the total duration of evaluated symbols $T_F$ given by $T_F = MT$ for OFDM and $T_F = MTM_B$ for GFDM. However, a parametrization optimized for the GFDM waveform and its features can also be performed.

We have considered a mobile vehicular communications channel in the 24 GHz frequency range with a coherence bandwidth of $B_{C50\%} = 1953$ kHz [35], and we have chosen $N = 256$, $M = 32$ and $M_B = 41$. The CP duration of each block is the same as in OFDM, 2.25$\mu$s. The complete parametrization is shown in Table 2. The pulse-shaping filter used in the GFDM waveform is a raised-cosine (RC) filter with a roll-off factor of 0.5.

It is possible to see in Table 1 and Table 2 that the GFDM modulation presents a lower unambiguous range than that of OFDM, but still above the maximum value detectable by the radar [35]. In contrast, the unambiguous velocity is much higher.

### C. MEASUREMENTS

All measurements were done according to the modulation parameters presented in Table 1 (OFDM) and

**TABLE 2. GFDM system parameters.**

| PARAMETERS | SYMBOL | VALUE |
|---|---|---|
| Carrier frequency | $f_c$ | 24 GHz |
| Number of subcarriers | $N$ | 256 |
| Number of GFDM symbols | $M$ | 32 |
| Number of evaluated blocks | $M_B$ | 41 |
| Total signal bandwidth | $B$ | 113.92 MHz |
| Subcarrier spacing | $\Delta f$ | 445 kHz |
| GFDM elementary symbol duration | $T$ | 2.25 $\mu$s |
| Cyclic prefix duration | $T_{CP}$ | 2.25 $\mu$s |
| Total block duration | $T_{GFDM}$ | 74.25 $\mu$s |
| Duration of evaluated symbols | $T_F$ | 3 ms |
| Range resolution | $\Delta R$ | 1.316 m |
| Velocity resolution | $\Delta v$ | 2.171 m/s |
| Unambiguous range | $R_{max}$ | 337 m |
| Unambiguous velocity | $v_{max}$ | $\pm$ 1424 m/s |
| Modulation | | 4-QAM |

Table 2 (GFDM). Fig. 7 shows the resulting radar images for a single static target at a distance of 2 m. Fig. 7(a) refers to GFDM-MF without the intrinsic interference removal technique, Fig. 7(b) refers to GFDM-ZF, Fig. 7(c) refers to GFDM-PMF with the proposed intrinsic interference removal technique, and Fig. 7(d) refers to OFDM. The estimated range value for OFDM was 1.93 m and for all GFDM techniques was 1.94 m.

In Fig. 7, the intrinsic interference is evident in the GFDM-MF radar due to the presence of a great amount of visible background noise. In contrast, the GFDM-PMF radar achieves a performance equal to that of the OFDM radar, not presenting any remaining intrinsic interference. Finally, the GFDM-ZF radar removed the intrinsic interference but, due to the ZF processing, it also increased the noise level. We conclude, then, that the proposed GFDM-PMF processing is more appropriate for radar than GFDM-ZF and GFDM-MF. Moreover, we conclude that it is feasible to use non-orthogonal waveforms for radar functions: since the transmitted signal is known by the radar system, it is possible to estimate the intrinsic interference and cancel the effects during the radar processing.

Throughout the rest of this paper, all further measurements related to the GFDM waveform will use the proposed GFDM-PMF radar processing technique.

Fig. 8 shows the measurements performed with OFDM and GFDM in the scenario with two static targets: one at 1.5 m and the other at 3.7 m. In the radar images, it is possible to verify that GFDM also presents the same performance as OFDM for multiple targets. The estimated range values for GFDM are 1.50 m and 3.67 m, and for OFDM 1.60 m and 3.60 m.

The scenario of a single static target at 2 m was also used to measure the inter-system interference in a multi-user environment. Fig. 9 shows the radar image for a system with an interference level in the reception (before filtering) of $SIR_{in} = -20$ dB for the OFDM and GFDM waveforms. In this figure, it is possible to see that the high OOB emission of OFDM causes a higher inter-system interference, resulting in a higher level of background noise (interference) in the

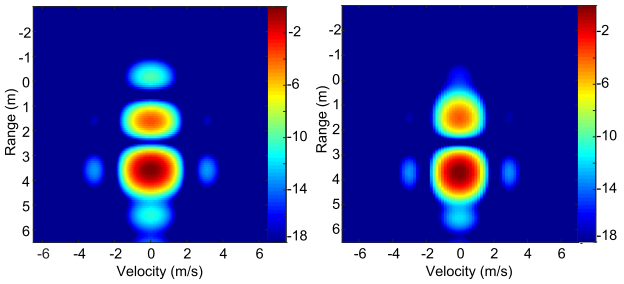


**FIGURE 8. Radar image with two targets for (a) OFDM and (b) GFDM.**

radar image. This may cause difficulties in detecting targets with low power signals reflected in a scenario with a large number of radars. On the other hand, since the background interference in the GFDM radar image is much lower, it is expected that in a scenario with multiple radars we are still close to a noise-limited system and targets are detected with much higher probability than in OFDM. We conclude, then, that the GFDM waveform is more appropriate for multi-user RadCom systems than the OFDM waveform.

## VI. PERFORMANCE EVALUATION

In this section, we compare the performance of the GFDM radar with that of the OFDM radar under various simulation environments with parameters presented in Table 1 (OFDM) and Table 2 (GFDM). First, we consider an environment with a single radar and multiple mobile targets. Then, we consider a noiseless environment with two radars (multiple users) and one target for the estimation of the inter-system interference after filtering in radar processing ($SIR_{out}$). The proposed GFDM-PMF processing technique was the one used for the GFDM radar. The transmitted data was randomly generated with a 4-QAM constellation.

### A. SINGLE USER – RANGE AND VELOCITY ESTIMATION

Three targets were considered with velocities of $v_1 = 4$ m/s, $v_2 = 2$ m/s and $v_3 = 3$ m/s, ranges of $R_1 = 8$ m, $R_2 = 10$ m and $R_3 = 5$ m, and normalized average power (to unity power) of the received signal in the ratios of $P_1 = 0.56$, $P_2 = 0.3$ and $P_3 = 0.14$. The channel was considered to be noiseless, flat, and with no attenuation.

A comparison between the GFDM and OFDM radars is presented in Fig. 10. Based on the results shown in this figure, it is possible to verify that the GFDM radar yields the same target velocity estimate as the OFDM radar.

### B. MULTIPLE USERS – INTER-SYSTEM INTERFERENCE

It is known that OFDM suffers from high OOB emissions and that one of the advantages of GFDM is its lower OOB emissions. It is for these reasons that the GFDM radar system has a much lower inter-system interference than the OFDM radar, as shown in the measurement results presented in Fig. 9.

In this section, the proposed GFDM radar is compared to the OFDM radar under the interference from another

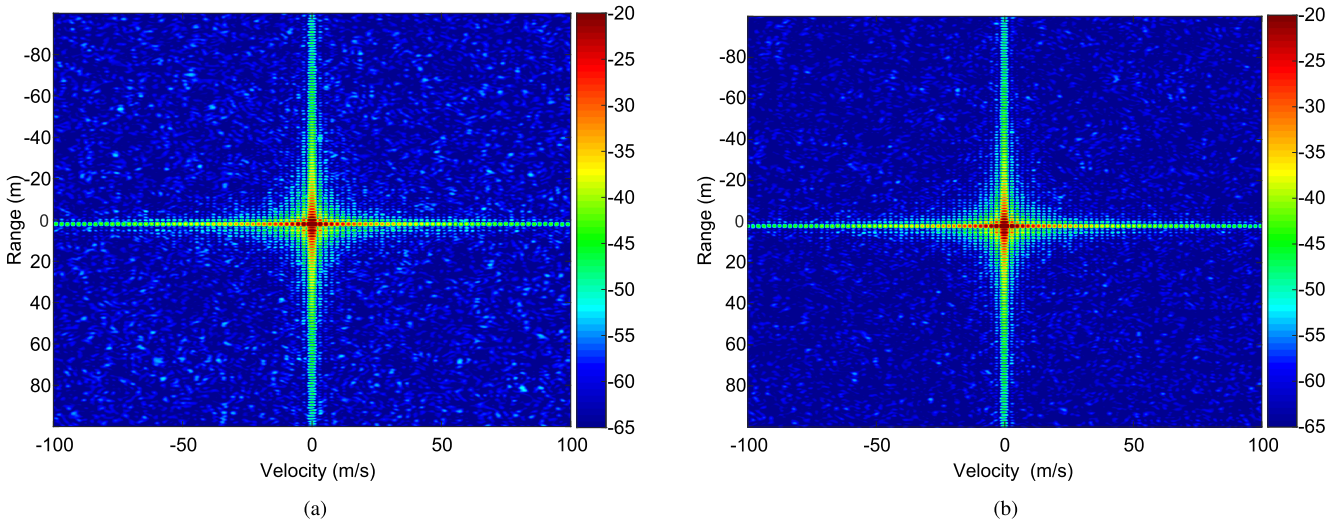


**FIGURE 9.** Radar image with inter-system interference for (a) OFDM and (b) GFDM.

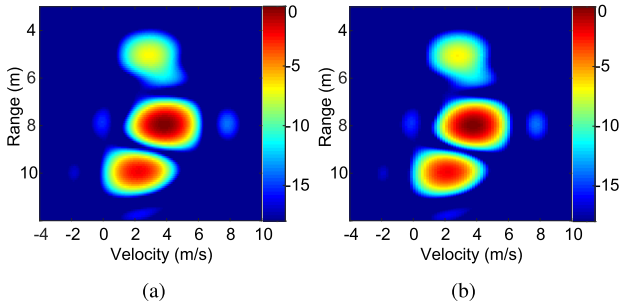


**FIGURE 10.** Comparison of the (a) GFDM and (b) OFDM radar image with multiple mobile targets.

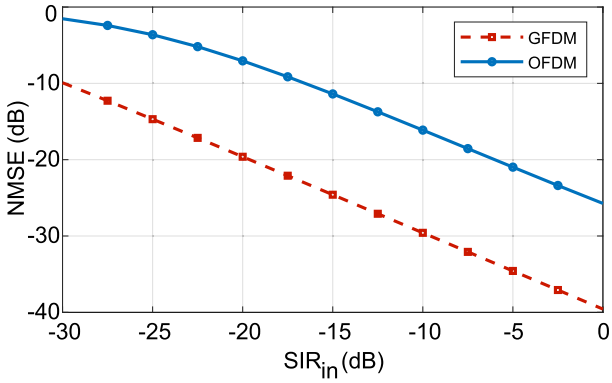


**FIGURE 11.** Variation of the NMSE of the received radar signal as a function of $SIR_{in}$.

radar with the same waveform in an adjacent channel (that is, OFDM interfered by OFDM and GFDM interfered by GFDM).

A configuration based on the modulation parameters presented in Table 1 (OFDM) and Table 2 (GFDM) is used. The radar system with carrier frequency $f_c$ is interfered by a radar with the same waveform with carrier frequency $f_c + B$. Both radars have the same bandwidth $B$. One target at a distance of $R = 2$ m and with a velocity $v = 0$ m/s is simulated considering a noiseless flat channel with no attenuation. After being received, the signal is filtered by a sharp low-pass filter with bandwidth $B$. In order to compare the performance of the GFDM and OFDM radars, we define the ratio between the power of the reflected radar signal and the power of the interfering signal as the signal-to-interference ratio (SIR), given by

$$SIR = \frac{P_{radar}}{P_{int}}, \tag{29}$$

where $P_{radar}$ is the power of the reflected radar signal and $P_{int}$ is the power of the interfering signal. We denote $SIR_{in}$ as the SIR of the received radar signal before filtering, and $SIR_{out}$ as the SIR of the received radar signal after filtering.

Moreover, the performance is also compared in terms of the normalized mean square error (NMSE) of the received radar signal after filtering in relation to the signal received by a radar with no interference, defined by

$$NMSE = \frac{\|\mathbf{Y}_{int} - \mathbf{Y}_{true}\|_2^2}{\|\mathbf{Y}_{true}\|_2^2}, \tag{30}$$

where $\mathbf{Y}_{true}$ is the received radar signal with no interference and $\mathbf{Y}_{int}$ is the signal with interference.

Fig. 11 shows the NMSE of the reconstructed signals for the OFDM and GFDM radars for different values of $SIR_{in}$. Greater interference can be observed in the OFDM radar due to its higher OOB emissions. Fig. 12 shows the interference after filtering ($SIR_{out}$) for both radars, with the GFDM radar presenting a $SIR_{out}$ better by approximately 9 dB than that of the OFDM radar.

In Fig. 12 we also compare the same systems with the addition of guard bands ($N_{GB} = N/32$). This figure demonstrates that, naturally, the two radars show an improvement in $SIR_{out}$ when guard bands are used. However, we note that the OFDM

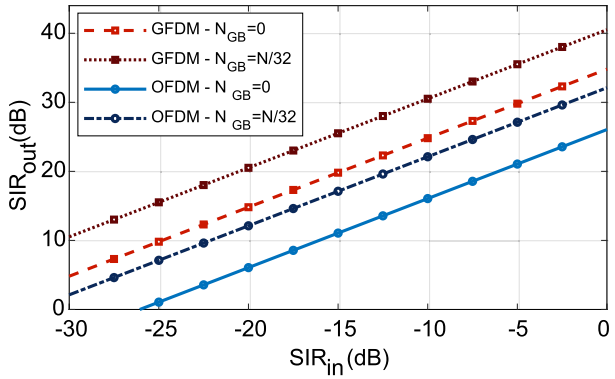


**FIGURE 12.** Variation of the post-filtered SIR as a function of $SIR_{in}$.

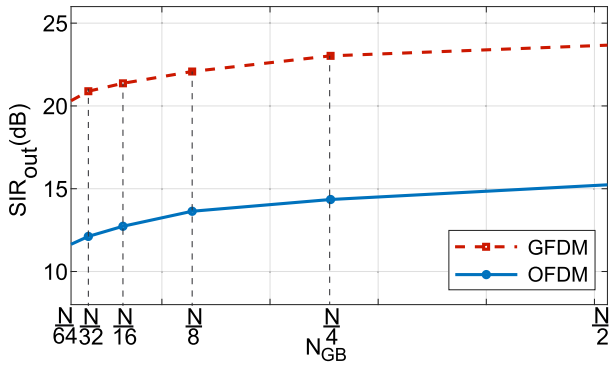


**FIGURE 13.** Variation of the pos-filtered SIR as a function of the guard bandwidth for $SIR_{in} = -20 = \text{dB}$.

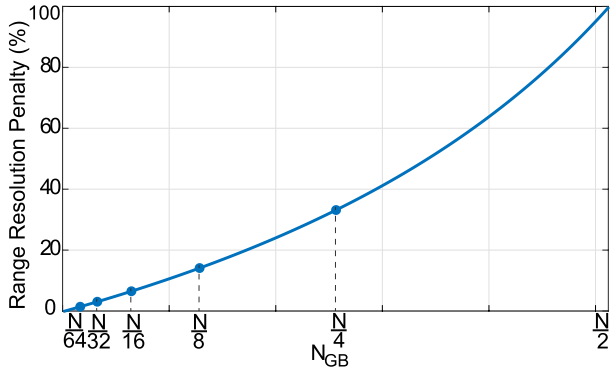


**FIGURE 14.** Relative decrease in range resolution as a function of the guard bandwidth.

radar with $N_{GB} = N/32$ still has more interference than the GFDM radar without guard bands.

In fact, for the OFDM radar to reach values of $SIR_{out}$ close to the GFDM radar's, it requires much wider guard bands. This is shown in Fig. 13, where a comparison of the $SIR_{out}$ versus the guard bandwidth is done for both radar systems (for $SIR_{in} = -20$ dB).

It can be seen from Fig. 13 that, although the GFDM radar only requires $N_{GB} = N/64$ to achieve $SIR_{out} = 20$ dB, the OFDM radar requires at least $N_{GB} = N/2$ to achieve $SIR_{out} = 15$ dB. The larger number of guard band subcarriers for OFDM causes not only a decrease in spectral efficiency for data transmission, but also a decrease in radar resolution capacity. Fig. 14 shows the relationship between the number of guards band subcarriers and the radar range resolution penalty, given by:

$$\Delta R \text{ Penalty}(\%) = \frac{\Delta R_{[N_{GB}]} - \Delta R_{[N_{GB}=0]}}{\Delta R_{[N_{GB}=0]}} * 100. \quad (31)$$

In order to achieve levels of $SIR_{out}$ equal to 20 dB and 15 dB respectively, the GFDM radar with a guard band of $N/32$ subcarriers would incur a range resolution penalty of only 1.6% ($\Delta R_{[N_{GB}=0]} = 1.316$ m and $\Delta R_{[N_{GB}=N/64]} = 1.336$ m) while the OFDM radar would incur a penalty of 100% ($\Delta R_{[N_{GB}=0]} = 1.316$ m and $\Delta R_{[N_{GB}=N/512]} = 2.632$ m).

## VII. CONCLUSION

This paper presents the processing of the GFDM waveform for radar with simulations and measurements at 24 GHz. The results demonstrate the viability of GFDM for RadCom systems, which combine radar and communications functions. In this paper, we also demonstrate that the proposed processing of GFDM using the matched filter at the receiver (GFDM-PMF) results in superior radar performance compared to using zero forcing. In fact, the intrinsic interference caused by the non-orthogonality of the GFDM subcarriers is completely mitigated by using the proposed GFDM radar processing technique. It was also verified that in multi-user environments, where interference between users in adjacent channels may occur, the GFDM radar presents less inter-system interference than the OFDM radar. Thus, the GFDM radar requires a narrower guard band and has a better range resolution than the OFDM radar, which makes the GFDM waveform a better candidate for RadCom systems. In this paper, we also show that, with correct processing, non-orthogonality in multicarrier waveforms is not a problem for radar estimation. This opens the door to further investigations with other non-orthogonal waveforms for RadCom systems. Research with multicarrier waveforms that optimize performance on both integrated functions (radar and data communication) will be performed.

## APPENDIX

The proposed method was based on the mathematics of the techniques demonstrated in [37]–[39]. The parameters $\Delta f$ and $T$ for GFDM radar are chosen so that the channel can be considered slow-fading in time and frequency, that is, constant during the duration of a symbol and the bandwidth of a subcarrier. We assume that the prototype filter $p(k)$ has a length much longer than the maximum delay spread of the channel, and is well-localized in time and frequency domains [39]. The channel frequency response at the $n$-th subcarrier and $m$-th symbol is denoted by $H_{n,m}$. The transmitted GFDM signal can be represented as

$$x(k) = \sum_{m=0}^{M-1} \sum_{n=0}^{N-1} S(n, m) p_{n,m}[k]. \quad (32)$$

and the received signal $y(k)$ as [37]

$$y(k) \approx \sum_{m=0}^{M-1} \sum_{n=0}^{N-1} H_{n,m} S(n,m) p_{n,m}[k] + \eta(k). \quad (33)$$

In the receiver, to demodulate the signal, a matched filtering is performed. Let $n_0$ be the index of a given subcarrier and $m_0$ the index of a given symbol, Then since $\{p_{n,m}[k] \circledast p^*_{n_0,m_0}[-k]\}|_{k=0} = \left(\mathbf{p}_{n_0,m_0}\right)^H \mathbf{p}_{n,m}$, the received data symbol $\hat{\mathbf{S}}$ at the $(n_0, m_0)$ position is

$$\hat{S}(n_0, m_0) = \{y(k) \circledast p^*_{n_0,m_0}[-k]\}|_{k=0}. \quad (34)$$

Because of the non-orthogonality of GFDM, intercarrier and intersymbol interference is present at the output of the GFDM demodulator when using matched filtering. The intrinsic interference induced from $N$ subcarriers and $M$ symbols on the $n_0$-th subcarrier of the $m_0$-th symbol can be expressed as

$$\zeta(n_0, m_0) = \sum_{m=0}^{M-1} \sum_{n=0}^{N-1} S(n,m)\{p_{n,m}[k] \circledast p^*_{n_0,m_0}[-k]\}|_{k=0}, \quad \text{for } (n,m) \neq (m_0, n_0). \quad (35)$$

Then, the received data symbol at the $(m_0, n_0)$ position can be rewritten as [39]

$$\hat{S}(n_0, m_0) = H_{n_0,m_0}\{S(n_0, m_0) + \zeta(n_0, m_0)\} + \tilde{\eta}(n_0, m_0). \quad (36)$$

In GFDM-PMF, considering $\hat{S}^{\dagger}_{PMF}(n_0, m_0) = \hat{S}(n_0, m_0)$, the element $(n_0, m_0)$ of the channel transfer matrix $\mathbf{D}$ is estimated as $D(n_0, m_0) = \hat{S}^{\dagger}_{PMF}(m_0, n_0)/S^{\dagger}_{PMF}(m_0, n_0)$, where $S^{\dagger}_{PMF}(n_0, n_0)$ is defined as

$$\begin{aligned} &S^{\dagger}_{PMF}(n_0, m_0) \\ &= \left\{ \left( \sum_{m=0}^{M-1} \sum_{n=0}^{N-1} S(n,m) p_{n,m}[k] \right) \circledast p^*_{n_0,m_0}[-k] \right\} |_{k=0} \quad (37) \\ &= S(n_0, m_0) + \sum_{m=0}^{M-1} \sum_{n=0}^{N-1} S(n,m)\{p_{n,m}[k] * p^*_{n_0,m_0}[-k]\}|_{k=0} \\ &= S(n_0, m_0) + \zeta(n_0, m_0). \quad (38) \end{aligned}$$

Thus, when performing the elementary division, we compensate the intrinsic interference in the radar transfer matrix:

$$\begin{aligned} D(n_0, m_0) &= \frac{\hat{S}^{\dagger}_{PMF}(n_0, m_0)}{S^{\dagger}_{PMF}(n_0, m_0)} \\ &= \frac{H_{n_0,m_0}\left(S(n_0, m_0) + \zeta(n_0, m_0)\right) + \tilde{\eta}(n_0, m_0)}{S(n_0, m_0) + \zeta(n_0, m_0)}. \end{aligned} \quad (39)$$

## REFERENCES

[1] J. E. Palmer, H. A. Harms, S. J. Searle, and L. Davis, "DVB-T passive radar signal processing," *IEEE Trans. Signal Process.*, vol. 61, no. 8, pp. 2116–2126, Apr. 2013.
[2] M. K. Bączyk, P. Samczynski, P. Krysik, and K. Kulpa, "Traffic density monitoring using passive radars," *IEEE Aerosp. Electron. Syst. Mag.*, vol. 32, no. 2, pp. 14–21, Feb. 2017.
[3] L. Daniel, S. Hristov, X. Lyu, A. G. Stove, M. Cherniakov, and M. Gashinova, "Design and validation of a passive radar concept for ship detection using communication satellite signals," *IEEE Trans. Aerosp. Electron. Syst.*, vol. 53, no. 6, pp. 3115–3134, Dec. 2017.
[4] D. Garmatyuk, J. Schuerger, and K. Kauffman, "Multifunctional software-defined radar sensor and data communication system," *IEEE Sensors J.*, vol. 11, no. 1, pp. 99–106, Jan. 2011.
[5] J. R. Gutierrez del Arroyo and J. A. Jackson, "WiMAX OFDM for passive SAR ground imaging," *IEEE Trans. Aerosp. Electron. Syst.*, vol. 49, no. 2, pp. 945–959, Apr. 2013.
[6] D. Ciuonzo, A. De Maio, G. Foglia, and M. Piezzo, "Intrapulse radar-embedded communications via multiobjective optimization," *IEEE Trans. Aerosp. Electron. Syst.*, vol. 51, no. 4, pp. 2960–2974, Oct. 2015.
[7] S. D. Blunt, P. Yatham, and J. Stiles, "Intrapulse radar-embedded communications," *IEEE Trans. Aerosp. Electron. Syst.*, vol. 46, no. 3, pp. 1185–1200, Jul. 2010.
[8] D. Ciuonzo, A. De Maio, G. Foglia, and M. Piezzo, "Pareto-theory for enabling covert intrapulse radar-embedded communications," in *Proc. IEEE Radar Conf. (RadarCon)*, May 2015, pp. 0292–0297.
[9] F. Guidi, A. Guerra, and D. Dardari, "Personal mobile radars with millimeter-wave massive arrays for indoor mapping," *IEEE Trans. Mobile Comput.*, vol. 15, no. 6, pp. 1471–1484, Jun. 2016.
[10] P. Kumari, J. Choi, N. Gonzalez-Prelcic, and R. W. Heath, Jr., "IEEE 802.11ad-based radar: An approach to joint vehicular communication-radar system," *IEEE Trans. Veh. Technol.*, vol. 67, no. 4, pp. 3012–3027, Apr. 2018.
[11] N. Levanon, "Multifrequency complementary phase-coded radar signal," *IEE Proc.-Radar, Sonar Navigat.*, vol. 147, no. 6, pp. 276–284, Dec. 2000
[12] B. J. Donnet and I. D. Longstaff, "Combining MIMO radar with OFDM communications," in *Proc. Eur. Radar Conf.*, Sep. 2006, pp. 37–40.
[13] C. Sturm and W. Wiesbeck, "Waveform design and signal processing aspects for fusion of wireless communications and radar sensing," *Proc. IEEE*, vol. 99, no. 7, pp. 1236–1259, Jul. 2011.
[14] A. Gameiro, D. Castanheira, J. Sanson, and P. P. Monteiro, "Research challenges, trends and applications for future joint radar communications systems," *Wireless Pers. Commun.*, vol. 100, no. 1, pp. 81–96, May 2018.
[15] C. Shi, F. Wang, M. Sellathurai, J. Zhou, and S. Salous, "Power minimization-based robust OFDM radar waveform design for radar and communication systems in coexistence," *IEEE Trans. Signal Process.*, vol. 66, no. 5, pp. 1316–1330, Mar. 2018.
[16] C. R. Berger, B. Demissie, J. Heckenbach, P. Willett, and S. Zhou, "Signal processing for passive radar using OFDM waveforms," *IEEE J. Sel. Topics Signal Process.*, vol. 4, no. 1, pp. 226–238, Feb. 2010.
[17] S. Sen and A. Nehorai, "Adaptive OFDM radar for target detection in multipath scenarios," *IEEE Trans. Signal Process.*, vol. 59, no. 1, pp. 78–90, Jan. 2011.
[18] G. Lellouch, A. K. Mishra, and M. Inggs, "Stepped OFDM radar technique to resolve range and Doppler simultaneously," *IEEE Trans. Aerosp. Electron. Syst.*, vol. 51, no. 2, pp. 937–950, Apr. 2015.
[19] S. Sen and A. Nehorai, "OFDM MIMO radar with mutual-information waveform design for low-grazing angle tracking," *IEEE Trans. Signal Process.*, vol. 58, no. 6, pp. 3152–3162, Jun. 2010.
[20] H. Rohling, *OFDM: Concepts for Future Communication Systems* (Signals and Communication Technology). Berlin, Germany: Springer, 2011.
[21] R. Gerzaguet, N. Bartzoudis, L. G. Baltar, V. Berg, J.-B. Doré, D. Kténas, O. Font-Bach, X. Mestre, M. Payaró, M. Färber, and K. Roth, "The 5G candidate waveform race: A comparison of complexity and performance," *EURASIP J. Wireless Commun. Netw.*, vol. 2017, no. 1, p. 13, Jan. 2017.
[22] X. Zhang, L. Chen, J. Qiu, and J. Abdoli, "On the waveform for 5G," *IEEE Commun. Mag.*, vol. 54, no. 11, pp. 74–80, Nov. 2016.
[23] P. Banelli, S. Buzzi, G. Colavolpe, A. Modenini, F. Rusek, and A. Ugolini, "Modulation formats and waveforms for 5G networks: Who will be the heir of OFDM?: An overview of alternative modulation schemes for improved spectral efficiency," *IEEE Signal Process. Mag.*, vol. 31, no. 6, pp. 80–93, Nov. 2014.
[24] S. Koslowski, M. Braun, and F. K. Jondral, "Using filter bank multicarrier signals for radar imaging," in *Proc. IEEE/ION Position, Location Navigat. Symp.*, May 2014, pp. 152–157.
[25] J. Sanson, A. Gameiro, D. Castanheira, and P. P. Monteiro, "24 GHz QAM-FBMC radar with communication system (RadCom)," in *Proc. Asia–Pacific Microw. Conf.*, Aug. 2018.
[26] A. Farhang, N. Marchetti, and L. E. Doyle, "Low-complexity modem design for GFDM," *IEEE Trans. Signal Process.*, vol. 64, no. 6, pp. 1507–1518, Mar. 2016.

[27] G. Fettweis, M. Krondorf, and S. Bittner, "GFDM—Generalized frequency division multiplexing," in *Proc. IEEE 69th Veh. Technol. Conf.*, Apr. 2009, pp. 1–4.
[28] D. Zhang, M. Matthé, L. L. Mendes, and G. Fettweis, "A study on the link level performance of advanced multicarrier waveforms under MIMO wireless communication channels," *IEEE Trans. Wireless Commun.*, vol. 16, no. 4, pp. 2350–2365, Apr. 2017.
[29] N. Michailow, I. Gaspar, S. Krone, M. Lentmaier, and G. Fettweis, "Generalized frequency division multiplexing: Analysis of an alternative multicarrier technique for next generation cellular systems," in *Proc. Int. Symp. Wireless Commun. Syst. (ISWCS)*, Aug. 2012, pp. 171–175.
[30] N. Michailow, M. Matthé, I. S. Gaspar, A. N. Caldevilla, L. L. Mendes, A. Festag, and G. Fettweis, "Generalized frequency division multiplexing for 5th generation cellular networks," *IEEE Trans. Commun.*, vol. 62, no. 9, pp. 3045–3061, Sep. 2014.
[31] M. Matthe, N. Michailow, I. Gaspar, and G. Fettweis, "Influence of pulse shaping on bit error rate performance and out of band radiation of generalized frequency division multiplexing," in *Proc. IEEE Int. Conf. Commun. Workshops (ICC)*, Jun. 2014, pp. 43–48.
[32] D. Zhang, L. L. Mendes, M. Matthé, I. S. Gaspar, N. Michailow, and G. P. Fettweis, "Expectation propagation for near-optimum detection of MIMO-GFDM signals," *IEEE Trans. Wireless Commun.*, vol. 15, no. 2, pp. 1045–1062, Feb. 2016.
[33] M. Matthé, L. L. Mendes, N. Michailow, D. Zhang, and G. Fettweis, "Widely linear estimation for space-time-coded GFDM in low-latency applications," *IEEE Trans. Commun.*, vol. 63, no. 11, pp. 4501–4509, Nov. 2015.
[34] D. Zhang, A. Festag, and G. P. Fettweis, "Performance of generalized frequency division multiplexing based physical layer in vehicular communications," *IEEE Trans. Veh. Technol.*, vol. 66, no. 11, pp. 9809–9824, Nov. 2017.
[35] M. Braun, C. Sturm, A. Niethammer, and F. K. Jondral, "Parametrization of joint OFDM-based radar and communication systems for vehicular applications," in *Proc. IEEE 20th Int. Symp. Pers., Indoor Mobile Radio Commun.*, Sep. 2009, pp. 3020–3024.
[36] N. A. Al-Hasaani, M. Namdar, and H. Ilhan, "Energy detection of spectrum sensing for cognitive radio networks using GFDM modulation," in *Proc. 10th Int. Conf. Electr. Electron. Eng.*, Nov. 2017, pp. 690–694.
[37] J.-P. Javaudin, D. Lacroix, and A. Rouxel, "Pilot-aided channel estimation for OFDM/OQAM," in *Proc. IEEE Veh. Technol. Conf. (VTC)*, vol. 3. Sep. 2003, pp. 1581–1585.
[38] C. Lélé, J.-P. Javaudin, R. Legouable, A. Skrzypczak, and P. Siohan, "Channel estimation methods for preamble-based OFDM/OQAM modulations," *Eur. Trans. Telecommun.*, vol. 19, no. 7, pp. 741–750, Jul. 2008.
[39] J. Choi, Y. Oh, H. Lee, and J. Seo, "Pilot-aided channel estimation utilizing intrinsic interference for FBMC/OQAM systems," *IEEE Trans. Broadcast.*, vol. 63, no. 4, pp. 644–655, Dec. 2017.

**JESSICA B. SANSON** received the M.Sc. degree in electronic engineering, with an emphasis on signal processing, from the Federal University of Rio de Janeiro, Brazil, in 2016, working in blind separation of sources and adaptive filtering. Her past research work includes research on space-time coding applied to a wireless communication. She is currently a student of the MAP-tele Doctoral Program in Telecommunications, a joint program between the University of Minho, the University of Aveiro, and the University of Porto. Her current research interests include developing signal processing techniques for a photonics-based networks, and integrating radar and communication functionalities.

**DANIEL CASTANHEIRA** received the Licenciatura (ISCED level 5) and Ph.D. degrees in electronics and telecommunications from the University of Aveiro, in 2007 and 2012, respectively, where he was an Assistant Professor with the Departamento de Eletrónica, Telecomunicações e Informática, in 2011. He is currently an Auxiliary Researcher with the Instituto the Telecomunicações, Aveiro, Portugal. He has been involved in several national and European Projects, namely RETIOT, SWING2, PURE-5GNET, HETCOP, COPWIN, and PHOTON, within the FCT Portuguese National Scientific Foundation, and CODIV, FUTON, and QOSMOS, with the FP7 ICT. His research interests include signal processing techniques for digital communications, with emphasis for physical layer issues including channel coding, precoding/equalization, and interference cancelation.

**ATÍLIO GAMEIRO** received the Licenciatura and Ph.D. degrees from the University of Aveiro, in 1985 and 1993, respectively. His industrial experience includes a period of one year at BT Labs and one year at NKT Elektronik. He is currently an Associate Professor with the Department of Electronics and Telecommunication, University of Aveiro, and a Researcher with the Instituto de Telecomunicações, Pólo de Aveiro, where he is a head of a group. His main interests include the signal processing techniques for digital communications and communication protocols, and within this research line, he has done work for optical and mobile communications, either at the theoretical and experimental level. He has published over 200 technical articles in international journals and conferences. He has been involved and has led IT or University of Aveiro participation on more than 20 national and European projects. His current research interests include space-time-frequency algorithms for the broadband wireless systems and cross-layer design.

**PAULO P. MONTEIRO** received the diploma Licenciatura in electronics and telecommunications engineering from the University of Aveiro, in 1988, the M.Sc. degree in electronic engineering from the University of Wales, U.K., in 1990, and the Ph.D. degree in electrical engineering from the University of Aveiro, in 1999, where he is currently an Associate Professor. He is also a Researcher with the Instituto de Telecomunicações. In 1992, he joined the Department of Electronic and Telecommunications Engineering, University of Aveiro, and the Optical Communications Group, Institute for Telecommunications, as an Assistant Professor and a Researcher, respectively. In 1999, he became an Auxiliary Professor at the University of Aveiro, and he was promoted to Associate Professor, in 2005. From October 2002 to March 2007, he was the Head of the Research of Optical Networks with Siemens S.A, Portugal. From April 2007 to December 2009, he was a Research Manager at transport, aggregation and fixed access with Nokia Siemens Networks (NSN), Portugal, where he was a R&D Manager of the Network Optimization unit, from January 2010 to June 2012, and a Research Manager, from July 2012 to May 2013. In May 2013, the Optical Networks business unit of Nokia Siemens Networks began operating as a new company Coriant, where he left in June 2013. He has authored/coauthored more than 18 patent applications and over 100 articles in journals and 360 conference contributions. His main research interests include optical communication networks, microwave photonic, and electronic subsystems. He is a member of ECOC 2018 Sub-Committee 5 on Photonic and Microwave Photonic Subsystems. He tutored and co-tutored successfully more than 14 PhD's, having participated in more than 28 projects (national and international). He was the Coordinator of a CELTIC project OPTRONET and a large-scale integrating project FUTON (FP7 ICT-2007-215533).